THE JOURNAL OF BIOLOGICAL CHEMISTRY VOL. 288, NO. 9, pp. 6754–6762, March 1, 2013

Hydrophobic Effect Drives Oxygen Uptake in Myoglobin via Histidine E7*[S]

Received for publication, October 6, 2012, and in revised form, January 4, 2013 Published, JBC Papers in Press, January 7, 2013, DOI 10.1074/jbc.M112.426056

Leonardo Boechi[‡1,2], **Mehrnoosh Arrar**[§1,3], **Marcelo A. Martí**[‡¶], **John S. Olson**[‖4], **Adrián E. Roitberg**[§5], **and Darío A. Estrin**[‡6]

From the [‡]*Departamento de Química Inorgánica, Analítica, y Química Física/Inquimae-Conicet, Facultad de Ciencias Exactas y Naturales, Universidad de Buenos Aires. Ciudad Universitaria, Pabellon 2, C1428EHA Buenos Aires, Argentina, the* [§]*Department of Chemistry and Quantum Theory Project, University of Florida, Gainesville, Florida 32611-7022, the* [¶]*Departamento de Química Biológica, Facultad de Ciencias Exactas y Naturales, Universidad de Buenos Aires, Ciudad Universitaria, Pabellon 2, C1428EHA Buenos Aires, Argentina, and the* [‖]*Department of Biochemistry and Cell Biology, Rice University, Houston, Texas 77005-1892*

Background: The distal histidine in myoglobin is thought to act as a gate regulating oxygen uptake.
Results: Neither the open nor closed conformation hinders oxygen uptake; a hydrophobic site is more apparent in the open conformation.
Conclusion: The driving force for ligand uptake is the hydrophobic effect.
Significance: This amplifies our understanding of the mechanisms through which proteins regulate ligand uptake.

Since the elucidation of the myoglobin (Mb) structure, a histidine residue on the E helix (His-E7) has been proposed to act as a gate with an open or closed conformation controlling access to the active site. Although it is believed that at low pH, the His-E7 gate is in its open conformation, the full relationship between the His-E7 protonation state, its conformation, and ligand migration in Mb is hotly debated. We used molecular dynamics simulations to first address the effect of His-E7 protonation on its conformation. We observed the expected shift from the closed to the open conformation upon protonation, but more importantly, noted a significant difference between the conformations of the two neutral histidine tautomers. We further computed free energy profiles for oxygen migration in each of the possible His-E7 states as well as in two instructive Mb mutants: Ala-E7 and Trp-E7. Our results show that even in the closed conformation, the His-E7 gate does not create a large barrier to oxygen migration and permits oxygen entry with only a small rotation of the imidazole side chain and movement of the E helix. We identify, instead, a hydrophobic site in the E7 channel that can accommodate an apolar diatomic ligand and enhances ligand uptake particularly in the open His-E7 conformation. This rate enhancement is diminished in the closed conformation. Taken together, our results provide a new conceptual framework for the histidine gate hypothesis.

In the crystal structures of hemoglobin (Hb)[7] and myoglobin (Mb) (1, 2), the histidine perched at the seventh position along the E helix resembles a gate guarding the entrance to the active site on the distal side of the heme group. Based on this observation, Perutz *et al.* (3) proposed that a swinging motion of this single amino acid side chain could control the migration rate for ligand entry into either Mb or Hb (Fig. 1), an idea that thus became known as the histidine gate hypothesis. More than 50 years of research have culminated in Mb becoming one of the most studied proteins in the field of structural biology (4). The histidine gate hypothesis and the role played by alternative ligand migration paths have been examined in detail by both experimental and theoretical methodologies but are still surrounded by controversy (5). It would be impractical to describe all the available data, and instead, we will attempt to summarize the key observations and discrepancies. Mb crystal structures have resolved the His-E7 side chain in the closed and open conformations (6). At neutral pH, the Mb crystal structures show the closed structure, which was originally observed by Perutz and Kendrew (1–3). Lowering the pH of Mb crystals resulted in His-E7 adopting an open conformation, which is attributed to His-E7 protonation and increased solvent exposure of imidazolium cation. Rabenstein *et al.* (7) analyzed the effect of pH on the His-E7 rotameric state theoretically and theirs results also indicated that when His-E7 is protonated the fraction of the open conformation increases.

The rates of ligand migration into and out of Mb are characterized experimentally by the overall ligand association (k'_X)

* This work was supported in part by the University of Buenos Aires, ANPCyT (PICT-25667), Consejo Nacional de Investigaciones Científicas y Técnicas, and the EU FP7 Program (Project NOStress).
[S] This article contains supplemental Movie 1.
[1] Present address: Dept. of Chemistry and Biochemistry, University of California, San Diego, La Jolla, CA 92093-0365.
[2] Supported in part by Consejo Nacional de Investigaciones Científicas y Técnicas and a Pew postdoctoral fellow.
[3] Supported in part by a Goldwater fellowship and subsequently by the National Science Foundation Graduate Research Fellowship.
[4] Supported by National Institutes of Health Grants HL047020 and GM035649 and Grant C-0612 from the Welch Foundation (Houston, TX).
[5] To whom correspondence may be addressed: Dept. of Chemistry and Quantum Theory Project, University of Florida, PO BOX 117200, Gainesville, FL 32611-7022. Tel.: 352-392-6972; Fax: 352-392-8722; E-mail: roitberg@ufl.edu.
[6] To whom correspondence may be addressed: Departamento de Química Inorgánica, Analítica, y Química Física/INQUIMAE-Consejo Nacional de Investigaciones Científicas y Técnicas, Facultad de Ciencias Exactas y Naturales, Universidad de Buenos Aires, Ciudad Universitaria, Pabellon 2, C1428EHA Buenos Aires, Argentina. Tel.: 54-11-4576-3378; Fax: 54-11-4576-3341; E-mail: dario@qi.fcen.uba.ar.

[7] The abbreviations used are: Hb, hemoglobin; Mb, myoglobin; MD, molecular dynamics.

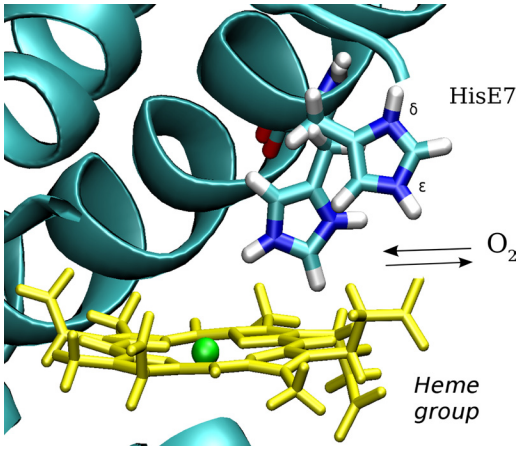

FIGURE 1. **A schematic representation of the His-E7 gate hypothesis, in which molecular oxygen can enter and exit the distal site due to the movement of the histidine at position 7 of helix E (His-E7).** The heme group (*yellow*) and His-E7 in the open and closed conformations are shown. The protonated state was chosen arbitrarily for schematic proposes.

and dissociation (k_X) rate constants, where X refers to the ligand being studied. The dissociation rate constant is determined by the speed of the iron-ligand bond breakage and the competition between the ligand migration to the solvent and internal rebinding to the iron atom. The limiting step is generally the iron-ligand bond breaking, with rates on the order of 0.01 to 100 s^{-1}, whereas rates of ligand migration out of the active site on the order of 10^6 to 10^7 s^{-1}, making the observed value of k_X a relatively poor indicator of ligand trajectories. The rate of ligand association is determined by the speed of ligand entry into the distal site and the extent of iron-ligand bond formation *versus* ligand escape and is often a more direct indicator of ligand pathways. Thus, for protein variants or changes in pH, observed changes in k'_X can be often be used to estimate changes in the initial barrier to the ligand entry (8–10). If the fraction of geminate recombination, F_{geminate}, is measured after photodissociation of the iron-ligand bond, the true bimolecular rate for ligand entry, k'_{entry}, can be computed as $k'_{\text{entry}} = k'_X / F_{\text{geminate}}$ because F_{geminate} provides the fraction of ligand molecules that bind to the iron atom after they enter the active site (8).

Site-directed mutagenesis studies in Mb have shown that both k'_{entry} and k'_X increase up to 10-fold when His-E7 is replaced with smaller apolar residues, such as Ala or Gly, whereas both rate constants decrease ~3-fold when His-E7 is replaced with the larger Trp (11), highlighting the importance of the E7 pathway in ligand migration. These results also show that the Trp-E7 and Ala-E7 Mb mutants are two useful limiting cases for evaluating the E7 pathway (8, 12). Association rate constants for ligand binding to Mb also suggest a pH dependence in the opening of the His-E7 gate because both k'_{O2} and k'_{CO} increase 2-fold upon lowering the pH from 7.0 to 4.6 (13, 14). This increase in the k'_X is more dramatic upon further lowering the pH to 2.0, but under these conditions, the increase in rate is due to protonation of the proximal histidine and formation of a four-coordinate deoxyheme group (15). In addition to the mutant and pH kinetic work, numerous other studies have also lent support to the relevance of the His-E7 gate opening to ligand entry in Mb (16–19).

TABLE 1
Summary of structures used to generate starting conformations for MD simulations

Mb variant	Protein Data Bank code
wt His-E7 (open conformation)	1SPE (6)[a]
wt His-E7 (closed conformation)	1VXF (6)
Ala-E7	102 M (16)
Trp-E7	3OGB (12)

[a] References are in parentheses.

Arguments against the His-E7 gate being the primary pathway for ligand entry come from studies showing the existence of multiple hydrophobic cavities (the Xe binding sites), which are thought to play a role in ligand migration, especially because internal pathways connecting the cavities have been identified (20–28). In addition, all computational studies have even identified many possible ligand exit pathways involving the Xe cavities (29–31), as well as ligand exit through the E7 gate (31). However, mutagenesis studies of Mb residues lining the Xe cavities only resulted in minor impacts on either k'_{O2} or k'_{entry} (8, 33), suggesting that the role of the Xe cavities in ligand uptake is likely secondary to that of the E7 pathway. Regardless of this controversy, there is a general consensus that the His-E7 gate is one of the principal pathways for ligand entry in myoglobin (11, 29, 30, 34).

Although correlations between pH, His-E7 conformation, and ligand migration rates have been identified, there is still a need for a thermodynamic characterization of ligand migration through the His-E7 gate and its relationship to the conformation of the imidazole side chain. To fill this gap, we performed molecular dynamics simulations to understand the relationships between the following: 1) the His-E7 protonation state and the side chain conformation (open or closed), 2) the open and closed conformations and the free energy barriers to oxygen movement, and 3) Ala-E7 and Trp-E7 substitutions and rates of ligand entry. To our knowledge, this study is the first to explicitly attempt to characterize the relationship between distal histidine tautomeric states, side chain orientations, amino acid replacement, and the free energy barriers for oxygen migration through the E7 channel.

MATERIALS AND METHODS

System Preparation—Classical molecular dynamics (MD) simulations were performed to sample the configurational space of the systems of study. Coordinates from the Protein Data Bank were used to create initial structural models (Table 1). Each conformation found in the crystal structures of the wild-type Mb (open and closed) was simulated in the three tautomeric states: the neutral δ-tautomer (HID), the neutral ϵ-tautomer (HIE), and the positively charged protonated state (HIP), giving us six different initial structures for the wild-type myoglobin.

Aside from His-E7, all histidine protonation states were assigned based on the immediate environment in the crystal structures and cross-checked against the protonation prediction server H++ (35). Throughout the simulations, all of the histidines maintained the same immediate environments, validating the choice of protonation states.

All systems were built using the Amber ff99SB force field (36) and solvated in a box of TIP3P water molecules, where the minimum distance between the protein and the extreme of

the box was 12 Å. Crystallographic waters were left as found in the original crystal structures. The heme parameters were determined using restrained electrostatic potential charges (37) and HF/6–31G(d) wave functions according to the Amber standard protocol, as described previously (38–45).

Molecular Dynamics Simulations—MD simulations were performed using the pmemd module within the AMBER11 simulation package. Periodic boundary conditions and Ewald sums were employed for the long range electrostatic interactions (46). With the SHAKE algorithm (47), we used a 2-fs time step for the propagation of coordinates in time in the isothermal-isobaric ensemble, using the Berendsen thermostat and barostat (48). The equilibration process was performed by slowly heating the system from 0 to 300 K over the course of 500 ps. We performed a total of 150 ns of MD simulations (isothermal-isobaric ensemble) for the HID and HIP system and 200 ns for the HIE system. To provide some evidence about the convergence the simulations, we used the last snapshot of each trajectory to perform (after an additional equilibration period) 50 ns of MD with switched protonation states: HIE to HID, HIE to HIP, HIP to HIE, and HID to HIE.

Multiple Steered Molecular Dynamics—In the multiple steered molecular dynamics method, the original potential is modified by adding an harmonic restraint called $V_{add}(t)$,

$$V_{add}(t) = \frac{1}{2}k[\xi - \xi_0(t)]^2 \qquad \text{(Eq. 1)}$$

where k is the spring constant, ξ is an arbitrary reaction coordinate, and $\xi_0(t)$ is the time-dependent center of the spring, which is modified based on an arbitrary velocity (v) as follows in Equation 2.

$$\xi_0(t) = \xi_i + vt \qquad \text{(Eq. 2)}$$

Using this approach and integrating the force applied in each step, it is possible to calculate the irreversible work (W) through the reaction coordinate chosen. From multiple irreversible works obtained starting from different initial microconfigurations it is possible to employ Jarzynski's equation (49) to estimate the free profile of the process. Jarzynski's equation relates the irreversible works with free energy change as follows,

$$e^{\frac{-\Delta G}{k_B T}} = \langle e^{\frac{-W}{k_B T}} \rangle \qquad \text{(Eq. 3)}$$

where k_B is the Boltzmann constant, T is the temperature, and W is the calculated irreversible work for each of the independent non-equilibrium process. A total of 40 independent perturbations were performed. This approach was used in a variety of studies such as ligand entry, escape, dynamic control of tunnel opening, and various mutagenesis studies, yielding results that are in excellent agreement with the experimentally determined rates (42–45, 50).

Because the reaction coordinate involves the formation of the O_2-iron bond, a process not allowed in the standard MD force field, we introduced a Morse potential to describe this coordination (51),

$$V(r) = D_o(1 - e^{(-\beta(r - r_0))^2}) \qquad \text{(Eq. 4)}$$

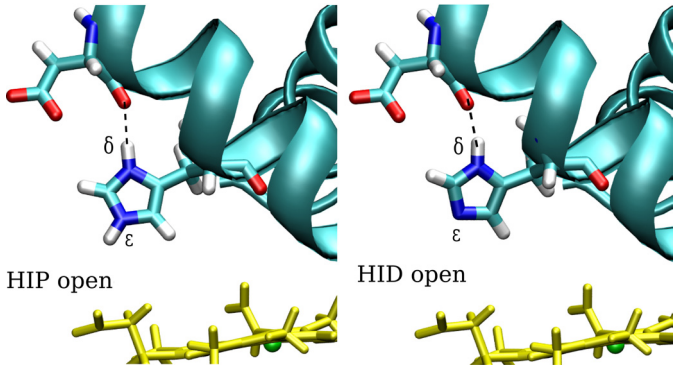

FIGURE 2. **Schematic representation of His-E7 neutral δ-tautomer (HID) and protonated (HIP) after MD simulations.** In both cases, His-E7 is in the open conformation forming a strong hydrogen bond with the carbonyl of Asp-60.

where D_o corresponds to the well depth (10 kcal/mol), r_0 is the equilibrium bond length (1.8 Å), and the parameter β was 4 $Å^{-1}$. Error analysis of the free energy profiles was done considering the bias inherent to the Jarzynski free energy estimator for a small number of independent simulations ($n = 40$) as proposed by Gore *et al.* (52).

RESULTS

Relationship between His-E7 Tautomeric and Conformational States—We performed extensive MD simulations to determine whether the His-E7 protonation state controls its conformation. To identify the protonation states of histidine, we use the following nomenclature: HIE, the neutral tautomer with the proton on the ϵ nitrogen; HID, the neutral tautomer with the proton on the δ nitrogen; and HIP, the histidine in its positively charged protonated state. As discussed below, the fixed protonation simulations afford an interesting analysis of the nonequivalence of the two neutral histidine tautomers. Given the two possible conformations of the imidazole side chain (open or closed), we performed a total of 150-ns MD simulations for each tautomer (HIE, HIP, HID) starting from the two possible conformations to remove any bias due to the initial structure. Moreover, we perturbed the protonation state after each 50-ns block of simulation time (HIE to HID, HIE to HIP, HIP to HIE, and HID to HIE) to ensure causality between the change in protonation state and the observed conformation of the His-E7 side chain. We classified the conformation as open or closed according to the His-E7 side chain dihedral angle (C-C_α-C_β-C_γ) (~160° open; ~60° closed) according to the observed values in the neutral and low pH Mb crystal structures as well as in previous MD studies (26). The results show that the protonated (HIP) and the neutral ϵ-tautomer (HIE) sample exclusively either the open or closed conformation, respectively (data not shown). The third form (HID), however, was found primarily in the open conformation, although not as exclusively as in the HIP form. In the HIP and HID forms, the open conformation is stabilized by a strong hydrogen bond interaction between the HN_δ of His-E7 and the backbone carbonyl group of nearby Asp-60 (Fig. 2), as previously observed (7, 53). Extending the gate analogy, this interaction serves as a "latch" for the His-E7 gate, maintaining it in the open conformation. Recall that the δ proton is present in both HIP and HID

but not in the HIE state. These results suggest that His-E7 does not have to necessarily be in its charged (protonated) state to sample the open conformation. Thus, even at neutral pH, Mb should significantly populate the open state even if it cannot be "seen" in crystal structures.

Structure and Dynamics of the Ala-E7 and Trp-E7 Mb Mutants—To have a better understanding of the steric constraints in the E7 channel, we also simulated the two experimentally well characterized Ala-E7 and Trp-E7 Mb mutants, which provide the upper and lower bounds for the rates of ligand entry (Table 2). Simulation of the Ala-E7 Mb mutant showed that the protein is stable with no observed changes in the distal site. The heme iron center is clearly accessible from the solvent, through the hole created by the absence of the E7 side chain (Fig. 3, *top-right panel*). The results for Trp-E7, on the other hand, were more surprising. The Trp-E7 side chain was drawn inward toward the distal site, as opposed to its initial outward conformation (Fig. 3, *bottom panel*, and Fig. 4). We observed a similar inward rotation of the hydrophobic side chain in the case of another mutant Phe-E7 Mb (data not shown). We should note that the new configuration adopted by Trp-E7 was previously observed in the crystal structures of the α Trp-E7 mutant subunit of human recombinant deoxyHbA containing wild-type β subunits (Fig. 4, *right panel*) (Protein Data Bank code 3NMM) (12). Both of the observed Trp-E7 conformations result in steric hindrance of the E7 pathway to the heme, as opposed to both Ala-E7 and the open His-E7 conformation (Fig. 3).

TABLE 2

Experimentally reported ligand entry rates of oxygen migration into Sperm whale myoglobin at pH 7.0

The bimolecular rate constant for ligand entry, k'_{entry}, was calculated as $k'_{O2}/F_{geminate}$ (8). The errors for wild-type (WT) myoglobin were estimated from averages of multiple geminate analyses (>10) (8).

Protein	k'_{O2} ($\mu M^{-1}\,s^{-1}$)	k'_{entry} ($\mu M^{-1}\,s^{-1}$)
wt	16 ± 3	34 ± 7
Ala-E7	53	410
Trp-E7	6,2	8.6

Oxygen Migration through the Conformation-dependent WT E7 Pathway—To characterize the oxygen entry process thermodynamically, we computed free energy profiles corresponding to the most populated conformation for each His-E7 state: the open conformation observed for HIP and HID and the closed conformation observed for HIE (Fig. 5). To compute each profile, we used multiple near-equilibrium perturbations and Jarzynski's equality (49, 50) to take dioxygen in the solvent, placed just outside the protein, and bring it to the bound state at 1.8 Å from the iron. The free energy was set to a value of 0 at 10 Å, where the oxygen molecule is fully solvated. The iron-O_2 interaction was modeled using a Morse potential to avoid spurious steric repulsion when the oxygen is within bonding distance of the iron. This strategy has been successfully applied to the determination of ligand binding to heme proteins by our group and others (51, 54–56).

The profiles for the open conformation (found in HIP and HID forms) present little or no barrier for oxygen entry into the E7 channel, which is characterized by a significant free energy

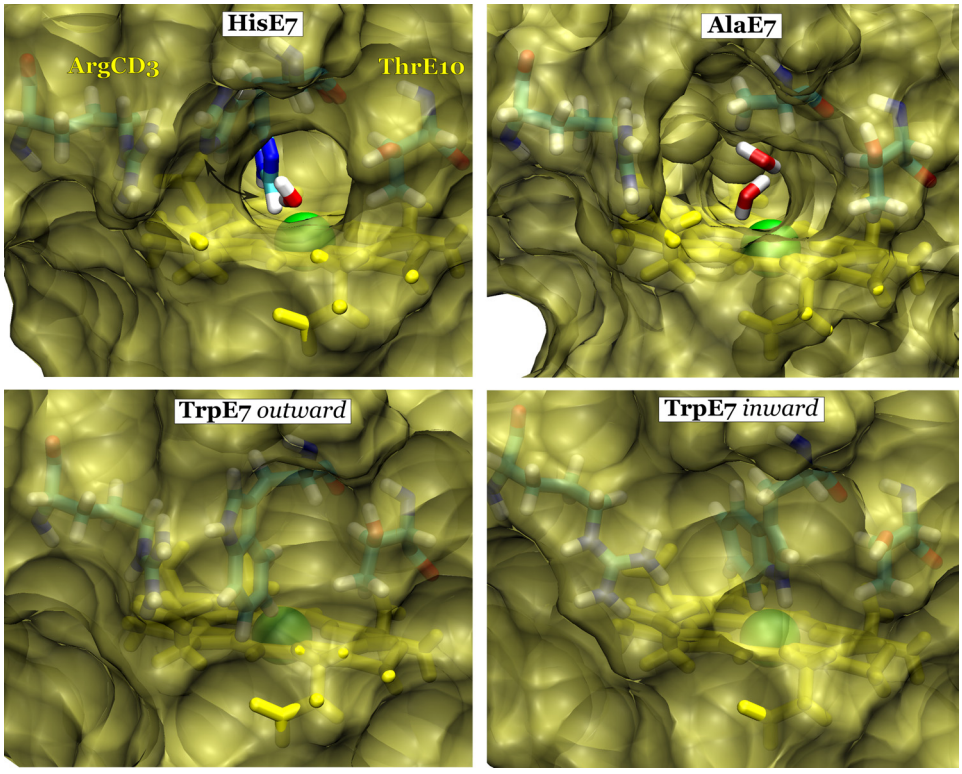

FIGURE 3. **Solvent-accessible surface contour of the E7 pathway.** The surface of wt Mb (*top left panel*) is shown with His-E7 in the open conformation with the closed His-E7 conformation superimposed in a stick representation for reference. Surface representations of mutants Ala-E7 Mb (*top right panel*), Trp-E7 in the outward conformation (*bottom left panel*) and Trp-E7 in the inward conformation (*bottom right panel*) are also shown. Clear tunnels for ligand migration can be seen in the open His-E7 conformation (*top left*) and in the Ala-E7 (*top right*) mutant, both of which can be occupied by water molecules (shown as sticks). The heme group (*yellow*), iron atom (*green*), and nearby residues (*cyan*) are depicted in each panel.

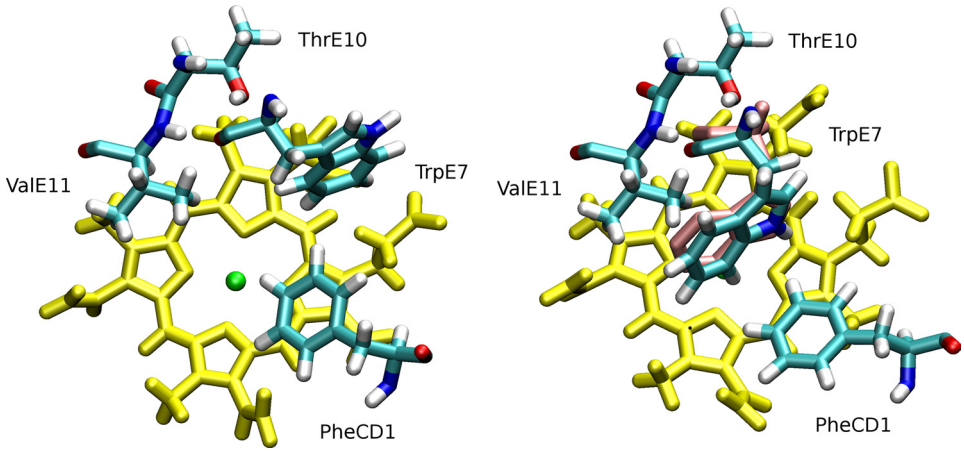

FIGURE 4. **Conformational switch of Trp-E7 from the outward conformation (*left panel*) to the inward conformation (*right panel*).** Trp-E7, Phe-CD1, Thr-E10, and Val-E11 are depicted in *cyan*. In both panels, the E7 pathway is blocked by the bulky Trp side chain (see Fig. 3). Position of Trp-E7 in the crystal structure of the Trp-E7 mutant α subunit of recombinant human hemoglobin with wild-type β subunit was superimposed in *violet* (Protein Data Bank code 3NMM) (12).

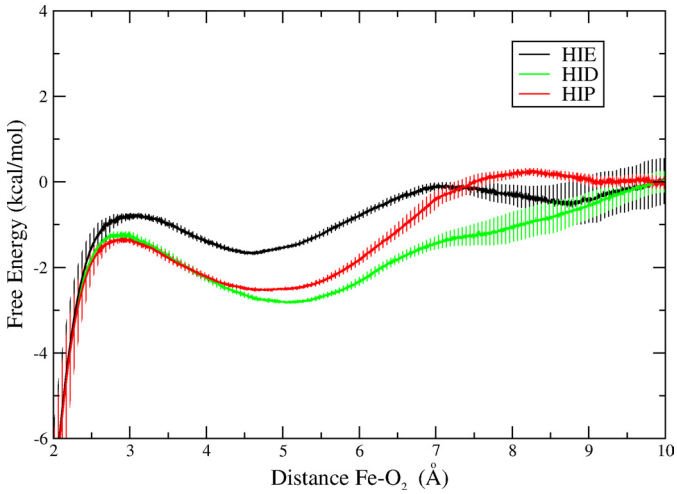

FIGURE 5. **Free energy profiles for ligand migration through the E7 pathway for the closed-HIE (*black*), open-HIP (*red*), and open-HID (*green*) conformations of the His-E7 in the wild-type Mb.** The free energy was set to a value of 0 at 10 Å, where the oxygen molecule is fully solvated. *Error bars* represent mean square error considering the bias inherent to the Jarzynski free energy estimator for a small number of independent simulations ($n = 40$) (52).

well at ~5 Å from the heme iron atom (Fig. 5). This well (~3 kcal/mol) corresponds to an apolar cavity just above the edge of the porphyrin ring, but still away from the iron-O_2 bond formation region. The ligand in this free energy well is in contact with apolar portions of the Thr-E10, His-E7 and Val-E11 side chains (Fig. 6). From this well, the oxygen does have to overcome a small barrier to be oriented just above the iron center for bond formation. The origin of this small barrier is the presence of Val-E11 (Fig. 6, *right panel*). Surprisingly, not even the closed conformation exhibits a significant barrier for oxygen entry into the E7 channel free energy well from the solvent (Fig. 5, *black curve*). As in the open conformation, there is only a small barrier to reach the iron, which in this case is due to the presence of Val-E11 and His-E7 (Fig. 6, *left panel*). The only notable difference between the closed and the open conformations is the depth of the free energy well, which is shallower in the closed conformation (~1.5 *versus* 3 kcal/mol). In the closed conformation of the His-E7 side chain, the imidazole ring occupies part of apolar channel that corresponds to the free energy well, sterically restricting O_2 in this pocket (Fig. 6, *left panel*).

Oxygen Entry through E7 Pathway in Trp-E7 and Ala-E7 Mb Mutants—The free energy profiles for Ala-E7 and Trp-E7 Mb provide an internal control of the methodology as well as a deeper understanding of the microscopic basis of the different ligand entry rate constants listed in Table 2. As expected, the profile for the Ala-E7 mutant exhibits absolutely no barrier for oxygen entry through the E7 channel. Surprisingly, the same free energy well, ~5 Å from the iron atom, is found in the channel of Ala-E7 Mb and is considerably deeper than in the wild type case, ~4 kcal/mol more favorable than bulk solvent (Fig. 7, *magenta curve*). The much smaller Ala side chain creates a larger and completely apolar cavity above the edge of the heme ring in which the oxygen molecule is more readily accommodated.

As described in the last section, the Trp-E7 Mb mutant was observed to sample two conformations in our simulations, including the one found in the Mb crystal structure (outward), and the one similar to that observed in the Trp-E7 α subunit of Hb mutant hybrid (inward). The resulting free energy profile for the outward but still blocked conformation of Trp-E7 shows a large ~3 kcal/mol barrier at 8 Å from the iron center (Fig. 7, *blue curve*). This barrier is directly related to the presence of the bulky Trp-E7 hindering access to the heme group (Figs. 3 and 4). In this case, the free energy well, which is 5 Å from the iron atom, is completely blocked. The inward conformation of Trp-E7 presents an even higher (~6 kcal/mol) barrier, which in this case is only 3 Å from the heme because the indole side chain has rotated into the distal pocket completely hindering access to the iron atom (Fig. 7, *orange curve*). The location of both barriers (outward and inward) corresponds to the shifted position of the Trp-E7 side chain in each case: at 8 Å from the iron center in the outward conformation and at 3 Å from the iron center in the inward conformation. The differences in heights are due to the mobility of the Trp-E7, which has more flexibility in the outward conformation, allowing the oxygen to circumvent the bulky side chain more easily than when it is in the inward conformation.

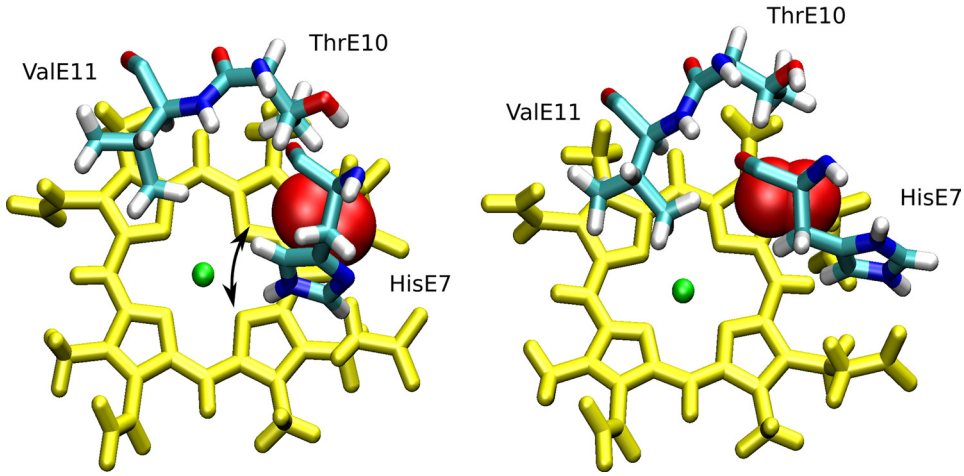

FIGURE 6. **Schematic representation of the apolar channel site corresponding to the free energy well for oxygen migration, which is ~5 Å from the iron in wt Mb.** In the *left panel*, His-E7 is in the closed conformation, perturbing the well, whereas in the *right panel*, it is open, leaving the well unrestricted for oxygen entry. Heme group (*yellow*) with iron atom (*green*) and relevant E7, E10 and E11 residues (*cyan*) are shown explicitly. The *arrow* indicates the small lateral movement that the His-E7 side chain and the E helix undergo to allow oxygen to migrate toward the iron in the closed conformation.

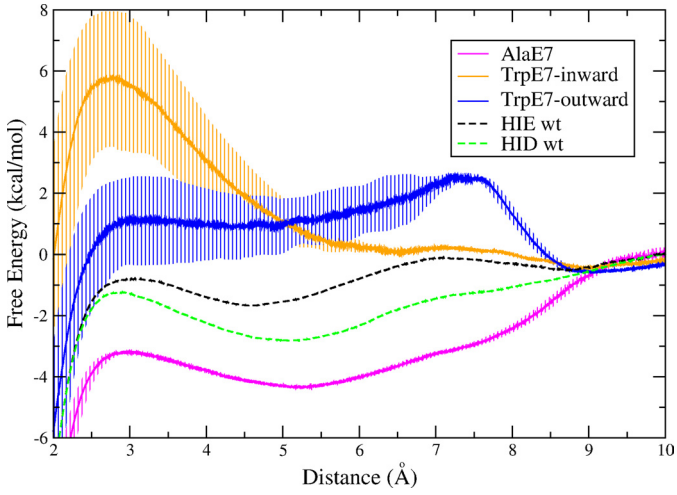

FIGURE 7. **Free energy profile of ligand migration through the E7 pathway for mutant proteins: Ala-E7 Mb (*magenta curve*), Trp-E7 Mb in the outward conformation as found in the crystal structure (*blue curve*) and Trp-E7 Mb in the inward conformation adopted during the simulation (*orange curve*).** The free energy was set to a value of 0 at 10 Å, where the oxygen molecule is fully solvated. *Error bars* represent mean square error considering the bias inherent to the Jarzynski free energy estimator for a small number of independent simulations ($n = 40$) (52). The free energy profile for WT HIE (*dashed black curve*) and HID (*dashed green curve*) from Fig. 5 are included as a reference.

DISCUSSION

The goal of the present study was to understand the relationship between the rate of ligand entry into Mb and the His-E7 side chain, specifically the E7 protonation, tautomerization, and conformation, as well as its replacement with larger and smaller functional groups. Simulation of the limiting case mutants Trp-E7 and Ala-E7 Mbs provided internal tests for the validity of our methodology and a clearer understanding of the ligand entry process. The pH-dependent conformational change of the His-E7 side chain and the open conformation of the HID tautomer highlights the contribution of the hydrogen bond between the δ proton of the imidazole group and the nearby Asp-60 carbonyl, which stabilizes the open conformation. Our theoretical results are in agreement with experimental crystallographic studies showing an increase in the open conformation upon lowering the pH. These simulations also underscore the importance of the amphipathic nature of the histidine residue, which allows it to adopt the open conformation, even in a neutral tautomeric state (HID) or, alternatively, serve as an interface between the hydrophobic site and solvent molecules in the HIE tautomeric state.

The Impact of the Apolar Free Energy Well in the E7 Channel—The most significant, and novel characteristic seen in the free energy profiles is the presence of a well located near the heme at ~5 Å from the iron. The well depth, relative to the free energy of O_2 in water, increases in the order: Trp-E7 (no distinguishable well) < His-E7-closed (~−1.5 kcal/mol) < His-E7-open (~−3 kcal/mol) < Ala-E7 (~−4 kcal/mol). The measured bimolecular rate constants for ligand entry, k'_{entry}, shown in Table 2 follow the opposite trend: Ala-E7 Mb > His-E7-open (low pH) Mb > His-E7-closed (neutral pH) Mb > Trp-E7 Mb. Thus, the depth of the free energy well is directly related to the ligand entry rate. The deeper free energy well can enhance the rate of ligand entry given that solvated oxygen crosses no large barrier to reach the apolar cavity or from the cavity to the distal site itself. One possible mechanistic interpretation involves pre-concentration of molecular oxygen (or other small ligands) in the apolar cavity, which would be more favorable when His-E7 is in the open conformation or replaced with smaller amino acids. In this interpretation, the overall bimolecular rate of entry into the distal pocket is given by the first order rate of ligand movement from the apolar cavity into the distal site times the fraction of O_2 molecules in the well. The latter fraction is very small and would be determined by $[O_2]/(K_{d,\text{cavity}} + [O_2]) \approx [O_2]/K_{d,\text{cavity}}$, where $K_{d,\text{cavity}}$ is the equilibrium dissociation constant for O_2 binding in the cavity. The approximation is reasonable because $K_{d,\text{cavity}}$ is a very large number on the order of 0.1 to 10 M(57), whereas $[O_2]$ in water equilibrated with 1 atm of air is ~0.00025 M. When the free energy well is made larger by the His-E7 to Ala mutation, $K_{d,\text{cavity}}$ will decrease, increasing the bimolecular rate of entry.

In a previous work studying oxygen uptake in the α chain of an Antarctic fish *Trematomus bernacchi* hemoglobin, using a

similar methodological approach, we also found that the closed conformation of His-E7 presents a very small free energy barrier to oxygen entry and that a free energy well at 5 Å is more prominent in the open conformation (38). Thus, although more exhaustive studies are needed, the conclusions from our simulations for ligand movement through the E7 channel seem to be valid for other globins with histidine in the E7 position as well.

The E7 Channel and Alternative Pathways—As mentioned in the Introduction, multiple pathways that do not involve the His-E7 gate have been proposed for ligand entry and exit in Mb. Such alternative migration pathways have been observed in other globins, such as in the *Mycobacterium tuberculosis* truncated Hb N (58–60) and in the *Cerebratulus lacteus* neuronal mini-globin (18), in which very clear apolar tunnels appear to be the main routes for ligand migration and not the E7 channel. In mammalian Mbs and Hbs, however, extensive experimental evidence has pointed to the E7 channel as the principal avenue for ligand migration (8, 11, 12, 18). Our calculated free energy profiles for both the open and closed His-E7 conformational states also lend considerable support to the E7 channel being a principal ligand migration route in Mb.

Comparison with Other Computational Studies—Previous simulation results of Mb have been interpreted to either support or discard the histidine gate hypothesis, based on the observed dynamics of His-E7. Bossa *et al.* (61) and Maragliano *et al.* (29) report the suspected opening of the His-E7 supporting the histidine gate hypothesis. On the other hand, some studies in both Hb and Mb report no opening motion of the His-E7 and raise doubt about the histidine gate hypothesis(32, 62). We believe that the difference between the results that lead to opposing conclusions may depend only on the tautomeric form of His-E7 used. The first set of authors used HID (mostly open in our simulations) and the second set used either HIE tautomer (exclusively closed) or did not comment on the protonation state. By considering all three forms of His-E7, we could differentiate between the conformational preference of each neutral tautomer (HID and HIE), which may reconcile some of the seemingly contradictory results above. The same exhaustive approach was used in earlier works by Jewsbury *et al.* (53) and more recently by Rabenstein *et al.* 7) leading to similar conclusions.

Regarding the ligand migration through the E7 channel, Cohen *et al.* report a free energy well at ~5–6 Å from the iron center (30), which may be the same that we identify in the HIP/HID profiles. A high barrier for ligand exit through the E7 channel was later reported by Maragliano *et al.* (29), where the HID state was used, supporting our computed free energy profile. The counterintuitive result where ligand escaped through the E7 pathway when the histidine is in the closed conformation has recently been observed for Hb, although it was interpreted as evidence against the histidine gate hypothesis (32). By considering free energy profiles for all the protonation/conformational states of His-E7, we show that although ligand entry may occur in the closed His-E7 conformation, the presence of a deeper free energy well in the open conformation enhances the uptake of oxygen, lending new support for the histidine gate hypothesis.

Conclusions—The natural image of a gate controlling the entry to a given place is that of a steric barrier when the gate is closed and then the absence of one when the gate is open. Our analysis showed little or no barrier for oxygen entry even in the closed His-E7 conformation. The opening of His-E7 does not significantly lower a barrier; rather, it vacates a hydrophobic cavity and results in a free energy well for small apolar ligands such as molecular oxygen. This analysis suggests that movement to the open conformation creates a favorable space for the entering ligand. Thus, the His-E7 conformation influences the thermodynamics of ligand migration through this pathway by creating a lower free energy pathway rather than altering a steric barrier.

The driving force for ligand uptake into this cavity is the hydrophobic effect, in which solvent water expels the apolar diatomic ligand toward the apolar cavity, which is more pronounced by outward movement of the imidazole side chain.

Acknowledgment—Supercomputing time was granted by the Large Allocations Resource Committee (TG-MCA05T010) and by supercomputing center of INQUIMAE - FCEyN/UBA.

REFERENCES

1. Perutz, M. F., Rossman, M. G., Cullis, A. F., Muirhead, H., Will, G., and North, A. C. (1960) Structure of haemoglobin: a three-dimensional Fourier synthesis at 5.5-A. resolution, obtained by x-ray analysis. *Nature* **185,** 416–422
2. Kendrew, J. C., Dickerson, R. E., Strandberg, B. E., Hart, R. G., Davies, D. R., Phillips, D. C., and Shore, V. C. (1960) Structure of myoglobin: A three-dimensional Fourier synthesis at 2 A2 resolution. *Nature* **185,** 422–427
3. Perutz, M. F., and Mathews, F. S. (1966) An x-ray study of azide methaemoglobin. *J. Mol. Biol.* **21,** 199–202
4. Frauenfelder, H., McMahon, B. H., and Fenimore, P. W. (2003) Myoglobin: the hydrogen atom of biology and a paradigm of complexity. *Proc. Natl. Acad. Sci. U.S.A.* **100,** 8615–8617
5. Elber, R. (2010) Ligand diffusion in globins: Simulations versus Experiment. *Curr. Opin. Struct. Biol.* **20,** 162–167
6. Yang, F., and Phillips, G. N. (1996) Crystal structures of CO-, deoxy- and met-myoglobins at various pH values. *J. Mol. Biol.* **256,** 762–774
7. Rabenstein, B., and Knapp, E. W. (2001) Calculated pH-dependent population and protonation of carbon-monoxy-myoglobin conformers. *Biophys. J.* **80,** 1141–1150
8. Scott, E. E., Gibson, Q. H., and Olson, J. S. (2001) Mapping the pathways for O_2 entry into and exit from myoglobin. *J. Biol. Chem.* **276,** 5177–5188
9. Milani, M., Pesce, A., Nardini, M., Ouellet, H., Ouellet, Y., Dewilde, S., Bocedi, A., Ascenzi, P., Guertin, M., Moens, L., Friedman, J. M., Wittenberg, J. B., and Bolognesi, M. (2005) Structural bases for heme binding and diatomic ligand recognition in truncated hemoglobins. *J. Inorg. Biochem.* **99,** 97–109
10. Ouellet, H., Milani, M., LaBarre, M., Bolognesi, M., Couture, M., and Guertin, M. (2007) The roles of Tyr(CD1) and Trp(G8) in Mycobacterium tuberculosis truncated hemoglobin O in ligand binding and on the heme distal site architecture. *Biochemistry* **46,** 11440–11450
11. Olson, J. S., Soman, J., and Phillips, G. N. (2007) Ligand pathways in myoglobin: a review of Trp cavity mutations. *IUBMB Life* **59,** 552–562
12. Birukou, I., Soman, J., and Olson, J. S. (2011) Blocking the gate to ligand entry in human hemoglobin. *J. Biol. Chem.* **286,** 10515–10529
13. Tian, W. D., Sage, J. T., and Champion, P. M. (1993) Investigations of ligand association and dissociation rates in the "open" and "closed" states of myoglobin. *J. Mol. Biol.* **233,** 155–166
14. Esquerra, R. M., Jensen, R. A., Bhaskaran, S., Pillsbury, M. L., Mendoza, J. L., Lintner, B. W., Kliger, D. S., and Goldbeck, R. A. (2008) The pH dependence of heme pocket hydration and ligand rebinding kinetics in

photodissociated carbonmonoxymyoglobin. *J. Biol. Chem.* **283,** 14165–14175
15. Coletta, M., Ascenzi, P., Traylor, T. G., and Brunori, M. (1985) Kinetics of carbon monoxide binding to monomeric hemoproteins. Role of the proximal histidine. *J. Biol. Chem.* **260,** 4151–4155
16. Smith, R. D., Blouin, G. C., Johnson, K. A., Phillips, G. N., Jr., and Olson, J. S. (2010) Straight-chain alkyl isocyanides open the distal histidine gate in crystal structures of myoglobin. *Biochemistry* **49,** 4977–4986
17. Blouin, G. C., Schweers, R. L., and Olson, J. S. (2010) Alkyl isocyanides serve as transition state analogues for ligand entry and exit in myoglobin. *Biochemistry* **49,** 4987–4997
18. Salter, M. D., Blouin, G. C., Soman, J., Singleton, E. W., Dewilde, S., Moens, L., Pesce, A., Nardini, M., Bolognesi, M., and Olson, J. S. (2012) Determination of ligand pathways in globins: apolar tunnels versus polar gates. *J. Biol. Chem.* **287,** 33163–33178
19. Schmidt, M., Nienhaus, K., Pahl, R., Krasselt, A., Anderson, S., Parak, F., Nienhaus, G. U., and Srajer, V. (2005) Ligand migration pathway and protein dynamics in myoglobin: A time-resolved crystallographic study on L29W MbCO. *Proc. Natl. Acad. Sci. U.S.A.* **102,** 11704–11709
20. Elber, R., and Karplus, M. (1990) Enhanced sampling in molecular dynamics: use of the time-dependent Hartree approximation for a simulation of carbon monoxide diffusion through myoglobin. *J. Am. Chem. Soc.* **112,** 9161–9175
21. Brunori, M., and Gibson, Q. H. (2001) Cavities and packing defects in the structural dynamics of myoglobin. *EMBO Rep.* **2,** 674–679
22. Bourgeois, D., Vallone, B., Schotte, F., Arcovito, A., Miele, A. E., Sciara, G., Wulff, M., Anfinrud, P., and Brunori, M. (2003) Complex landscape of protein structural dynamics unveiled by nanosecond Laue crystallography. *Proc. Natl. Acad. Sci. U.S.A.* **100,** 8704–8709
23. Tomita, A., Sato, T., Ichiyanagi, K., Nozawa, S., Ichikawa, H., Chollet, M., Kawai, F., Park, S. Y., Tsuduki, T., Yamato, T., Koshihara, S. Y., and Adachi, S. (2009) Visualizing breathing motion of internal cavities in concert with ligand migration in myoglobin. *Proc. Natl. Acad. Sci. U.S.A.* **106,** 2612–2616
24. Hummer, G., Schotte, F., and Anfinrud, P. A. (2004) Unveiling functional protein motions with picosecond x-ray crystallography and molecular dynamics simulations. *Proc. Natl. Acad. Sci. U.S.A.* **101,** 15330–15334
25. Lim, M., Jackson, T. A., and Anfinrud, P. A. (1997) Ultrafast rotation and trapping of carbon monoxide dissociated from myoglobin. *Nat. Struct. Biol.* 4, 209–214
26. Bossa, C., Amadei, A., Daidone, I., Anselmi, M., Vallone, B., Brunori, M., and Di Nola, A. (2005) Molecular dynamics simulation of sperm whale myoglobin: effects of mutations and trapped CO on the structure and dynamics of cavities. *Biophys. J.* **89,** 465–474
27. Ceccarelli, M., Anedda, R., Casu, M., and Ruggerone, P. (2008) CO escape from myoglobin with metadynamics simulations. *Proteins* **71,** 1231–1236
28. Ostermann, A., Waschipky, R., Parak, F. G., and Nienhaus, G. U. (2000) Ligand binding and conformational motions in myoglobin. *Nature* **404,** 205–208
29. Maragliano, L., Cottone, G., Ciccotti, G., and Vanden-Eijnden, E. (2010) Mapping the network of pathways of CO diffusion in myoglobin. *J. Am. Chem. Soc.* **132,** 1010–1017
30. Cohen, J., Arkhipov, A., Braun, R., and Schulten, K. (2006) Imaging the migration pathways for O2, CO, NO, and Xe inside myoglobin. *Biophys. J.* **91,** 1844–1857
31. Cohen, J., Olsen, K. W., and Schulten, K. (2008) Finding gas migration pathways in proteins using implicit ligand sampling. *Methods Enzymol.* **437,** 439–457
32. Shadrina, M. S., English, A. M., and Peslherbe, G. H. (2012) Effective simulations of gas diffusion through kinetically accessible tunnels in multisubunit proteins: O2 pathways and escape routes in T-state deoxyhemoglobin. *J. Am. Chem. Soc.* **134,** 11177–11184
33. Scott, E. E., and Gibson, Q. H. (1997) Ligand migration in sperm whale myoglobin. *Biochemistry* **36,** 11909–11917
34. Ruscio, J. Z., Kumar, D., Shukla, M., Prisant, M. G., Murali, T. M., and Onufriev, A. V. (2008) Atomic level computational identification of ligand migration pathways between solvent and binding site in myoglobin. *Proc. Natl. Acad. Sci. U.S.A.* **105,** 9204–9209
35. Gordon, J. C., Myers, J. B., Folta, T., Shoja, V., Heath, L. S., and Onufriev, A. (2005) H++: a server for estimating pKas and adding missing hydrogens to macromolecules. *Nucleic Acids Res.* **33,** W368–371
36. Hornak, V., Abel, R., Okur, A., Strockbine, B., Roitberg, A., and Simmerling, C. (2006) Comparison of multiple Amber force fields and development of improved protein backbone parameters. *Proteins* **65,** 712–725
37. Bayly, C. I., Cieplak, P., Cornell, W., and Kollman, P. A. (1993) A well-behaved electrostatic potential based method using charge restraints for deriving atomic charges: the RESP model. *J. Phys. Chem.* **97,** 10269–10280
38. Boechi, L., Martì, M. A., Vergara, A., Sica, F., Mazzarella, L., Estrin, D. A., and Merlino, A. (2011) Protonation of histidine 55 affects the oxygen access to heme in the alpha chain of the hemoglobin from the Antarctic fish *Trematomus bernacchii*. *IUBMB Life* **63,** 175–182
39. Martí, M. A., González Lebrero, M. C., Roitberg, A. E., and Estrin, D. A. (2008) Bond or cage effect: how nitrophorins transport and release nitric oxide. *J. Am. Chem. Soc.* **130,** 1611–1618
40. Martí, M. A., Bidon-Chanal, A., Crespo, A., Yeh, S. R., Guallar, V., Luque, F. J., and Estrin, D. A. (2008) Mechanism of product release in NO detoxification from *Mycobacterium tuberculosis* truncated hemoglobin N. *J. Am. Chem. Soc.* **130,** 1688–1693
41. Capece, L., Marti, M. A., Crespo, A., Doctorovich, F., and Estrin, D. A. (2006) Heme protein oxygen affinity regulation exerted by proximal effects. *J. Am. Chem. Soc.* **128,** 12455–12461
42. Boechi, L., Mañez, P. A., Luque, F. J., Marti, M. A., and Estrin, D. A. (2010) Unraveling the molecular basis for ligand binding in truncated hemoglobins: the trHbO *Bacillus subtilis* case. *Proteins* **78,** 962–970
43. Boechi, L., Martí, M. A., Milani, M., Bolognesi, M., Luque, F. J., and Estrin, D. A. (2008) Structural determinants of ligand migration in *Mycobacterium tuberculosis* truncated hemoglobin O. *Proteins* **73,** 372–379
44. Pesce, A., Nardini, M., Dewilde, S., Capece, L., Martí, M. A., Congia, S., Salter, M. D., Blouin, G. C., Estrin, D. A., Ascenzi, P., Moens, L., Bolognesi, M., and Olson, J. S. (2011) Ligand migration in the apolar tunnel of *Cerebratulus lacteus* mini-hemoglobin. *J. Biol. Chem.* **286,** 5347–5358
45. Bidon-Chanal, A., Martí, M. A., Crespo, A., Milani, M., Orozco, M., Bolognesi, M., Luque, F. J., and Estrin, D. A. (2006) Ligand-induced dynamical regulation of NO conversion in *Mycobacterium tuberculosis* truncated hemoglobin-N. *Proteins* **64,** 457–464
46. Jorgensen, W. L., Chandrasekhar, J., Madura, J. D., Impey, R. W., and Klein, M. L. (1983) Comparison of simple potential functions for simulating liquid water. *J. Chem. Phys.* **79,** 926–936
47. Ryckaert, J. P., Ciccotti, G., and Berendsen, H. (1977) Numerical integration of the cartesian equations of motion of a system with constraints: molecular dynamics of n-alkanes. *J. Comput. Phys.* **23,** 327–341
48. Berendsen, H. J. C., Postma, J. P. M., Van Gunsteren, W. F., DiNola, A., and Haak, J. R. (1984) Molecular dynamics with coupling to an external bath. *J. Chem. Phys.* **81,** 3684–3690
49. Jarzynski, C. (1997) Nonequilibrium Equality for Free Energy Differences. *Phys. Rev. Lett.* **78,** 2690–2693
50. Xiong, H., Crespo, A., Marti, M., Estrin, D., and Roitberg, A. E. (2006) Free Energy Calculations with Non-Equilibrium Methods: Applications of the Jarzynski Relationship. *Theor. Chem. Acc.* **116,** 338–346
51. Meuwly, M., Becker, O. M., Stote, R., and Karplus, M. (2002) NO rebinding to myoglobin: a reactive molecular dynamics study. *Biophys. Chem.* **98,** 183–207
52. Gore, J., Ritort, F., and Bustamante, C. (2003) Bias and error in estimates of equilibrium free-energy differences from nonequilibrium measurements. *Proc. Natl. Acad. Sci. U.S.A.* **100,** 12564–12569
53. Jewsbury, P., and Kitagawa, T. (1994) The distal residue-CO interaction in carbonmonoxy myoglobins: a molecular dynamics study of two distal histidine tautomers. *Biophys. J.* **67,** 2236–2250
54. De Biase, P. M., Paggi, D. A., Doctorovich, F., Hildebrandt, P., Estrin, D. A., Murgida, D. H., and Marti, M. A. (2009) Molecular basis for the electric field modulation of cytochrome *c* structure and function. *J. Am. Chem. Soc.* **131,** 16248–16256
55. Nadra, A. D., Martí, M. A., Pesce, A., Bolognesi, M., and Estrin, D. A. (2008) Exploring the molecular basis of heme coordination in human neuroglobin. *Proteins* **71,** 695–705
56. Capece, L., Marti, M. A., Bidon-Chanal, A., Nadra, A., Luque, F. J., and Estrin, D. A. (2009) High pressure reveals structural determinants for

globin hexacoordination: neuroglobin and myoglobin cases. *Proteins* **75,** 885–894
57. Birukou, I., Maillett, D. H., Birukova, A., and Olson, J. S. (2011) Modulating distal cavities in the α and β subunits of human HbA reveals the primary ligand migration pathway. *Biochemistry* **50,** 7361–7374
58. Wittenberg, J. B., Bolognesi, M., Wittenberg, B. A., and Guertin, M. (2002) Truncated hemoglobins: a new family of hemoglobins widely distributed in bacteria, unicellular eukaryotes, and plants. *J. Biol. Chem.* **277,** 871–874
59. Milani, M., Pesce, A., Ouellet, Y., Ascenzi, P., Guertin, M., and Bolognesi, M. (2001) *Mycobacterium tuberculosis* hemoglobin N displays a protein tunnel suited for O2 diffusion to the heme. *EMBO J.* **20,** 3902–3909
60. Cazade, P. A., and Meuwly, M. (2012) Oxygen migration pathways in NO-bound truncated hemoglobin. *Chemphyschem* **13,** 4276–4286
61. Bossa, C., Anselmi, M., Roccatano, D., Amadei, A., Vallone, B., Brunori, M., and Di Nola, A. (2004) Extended molecular dynamics simulation of the carbon monoxide migration in sperm whale myoglobin. *Biophys. J.* **86,** 3855–3862
62. Cohen, J., and Schulten, K. (2007) O2 migration pathways are not conserved across proteins of a similar fold. *Biophys. J.* **93,** 3591–3600